Biophysical Journal, Volume *112*

Supplemental Information

Volume Transitions of Isolated Cell Nuclei Induced by Rapid Temperature Increase

Chii J. Chan, Wenhong Li, Gheorghe Cojoc, and Jochen Guck

SUPPLEMENTARY MATERIAL

Volume transitions of isolated cell nuclei in response to rapid temperature increase
by C. J. Chan *et al.*

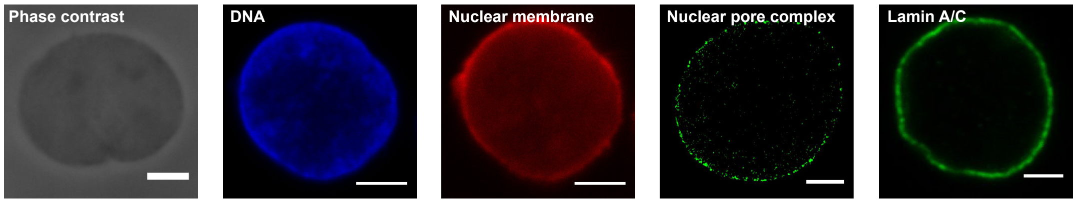

Fig. S1: Images of nuclear components in swollen state. Phase contrast and confocal images of isolated HL60 nuclei stained for DNA (Hoechst), membrane (FM4-64), nuclear pore complex (Mab414) and lamin A/C (anti-lamin A/C), in deionized water. Chromatin in DI appeared more decondensed than those in PBS, and preferentially located at the nuclear periphery. The nuclear pore complex (NPC) are preserved in the swollen state, as shown by the punctuated rim at the nuclear membrane. The NPCs appeared more sparsely distributed in swollen nuclei than those in PBS (see **Fig. 1a** in main text). Overall, the existence of a nuclear membrane, lamin and NPC indicate that the nuclear envelope for HL60 nuclei is intact even when heavily swollen. Scale bars 5 μm.

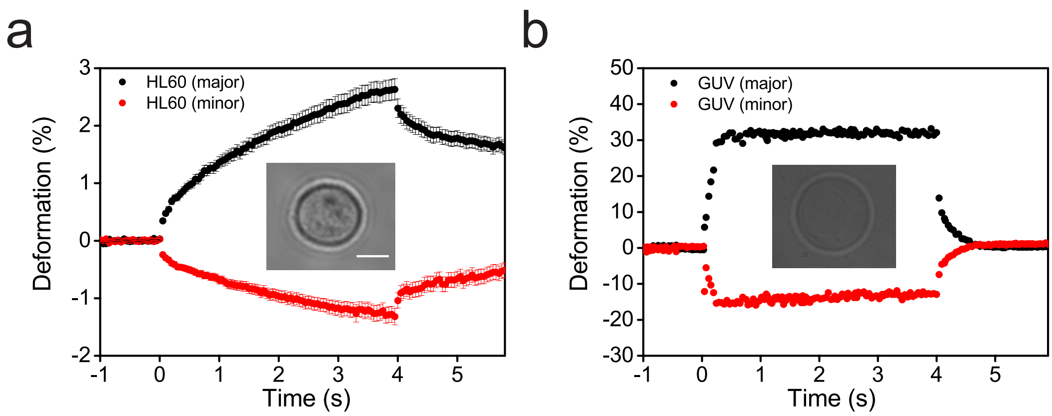

Fig. S2: Volume conservation for cells and giant unilamellar vesicles (GUVs) upon optical stretching in 780 nm OS in PBS prepared in deionized water. Average deformation profiles for **a**. HL60 cells (n = 54) and **b.** a representative GUV. Stretch power = 1.6 W, $\Delta T_{laser} \approx 3°C$. Negative deformation along minor axis (red) is approximately half that of the positive deformation along the major axis (black) in both cases, indicating volume conservation. HL60 cells showed more viscoelastic creep response while the GUVs appeared more elastic, which is also characterized by the immediate relaxation at the end of the stretch. Stretch period is from t = 0 to 4 s. Error bars represent SE. Scale bar 5 μm.

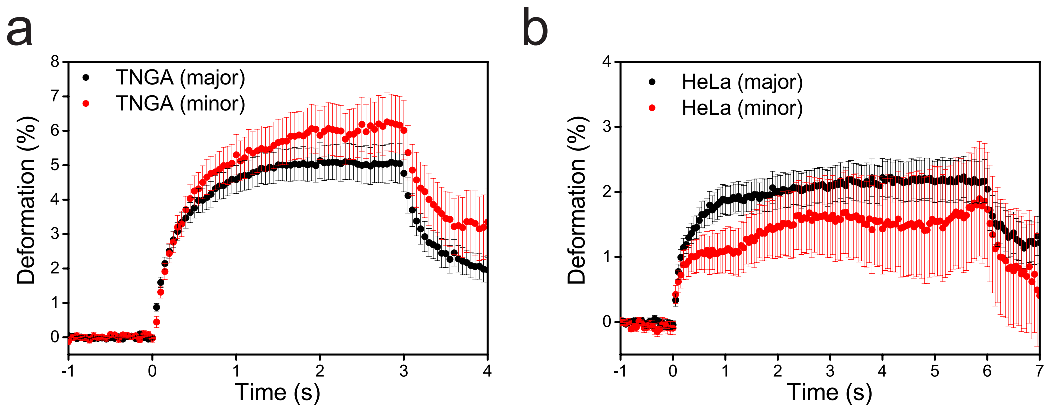

Fig. S3: Nuclear swelling in other cell types upon optical stretching in 1064 nm OS. a. Deformation curves for isolated TNGA mouse embryonic stem cell nuclei (n = 24), when stretched under 2.0 W ($\Delta T_{laser} \approx 22°C$), with stretch period from $t = 0$ to 3 s. **b**. Deformation curves for isolated HeLa nuclei (n = 60), when stretched with 1.4 W ($\Delta T_{laser} \approx 15°C$) between $t = 0$ to 6 s. Error bars represent SE.

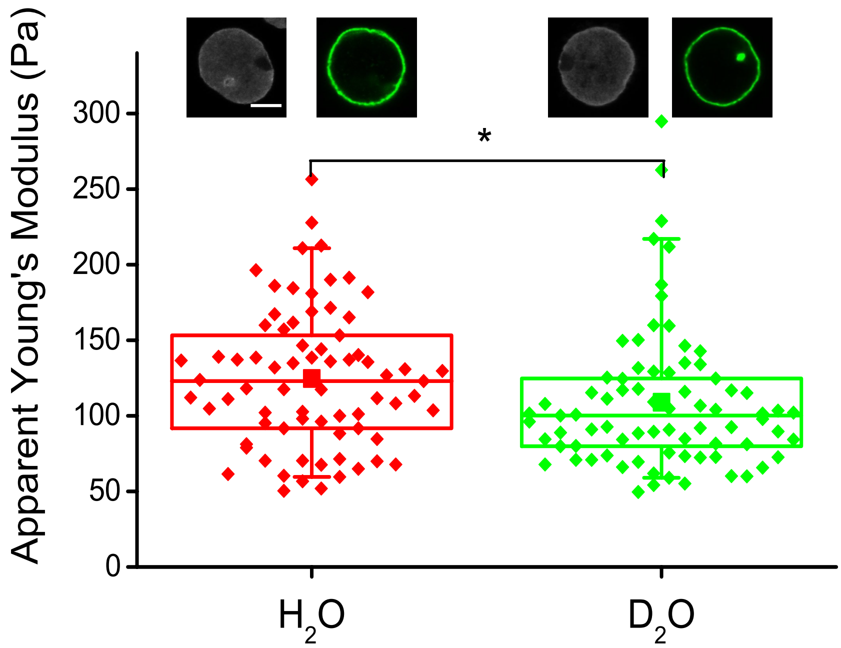

Fig. S4: AFM measurements of HL60 nuclei in 20% PBS prepared in heavy (D_2O) and deionized water (H_2O). There is only a minor difference (*$p < 0.05$) of the apparent Young's moduli between nuclei prepared with heavy water (n = 77) and deionized water (n = 73), suggesting that heavy water does not significantly change the nuclear stiffness. If any, they led to a slight reduction in nuclear stiffness, opposite to findings from OS studies. Inset depicts images of nuclei stained with DNA (grey) and lamin A/C (green), showing no visible difference in morphology and size of nuclei in heavy and deionized water. Scale bar 5 μm.

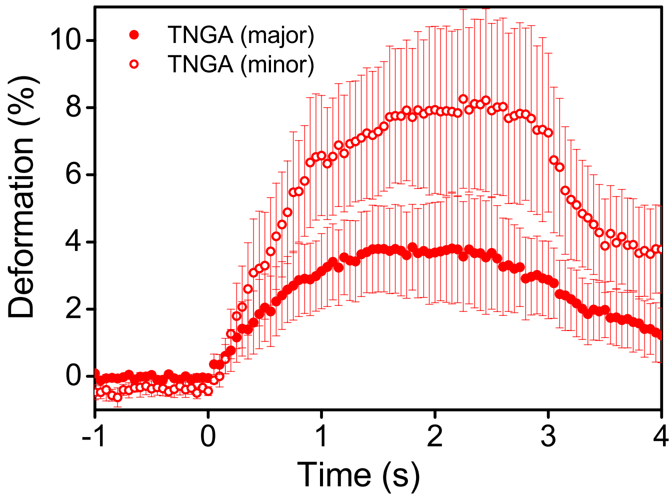

Fig. S5: Nuclear swelling upon laser heating by 1480 nm laser. TNGA nuclei (n = 16) in PBS were trapped by the 1064 nm OS and heated by a 1480 nm diode laser coupled to one of the 1064 nm optical fibers. Heating period is from $t = 0$ to 3 s. Error bars represent SE.

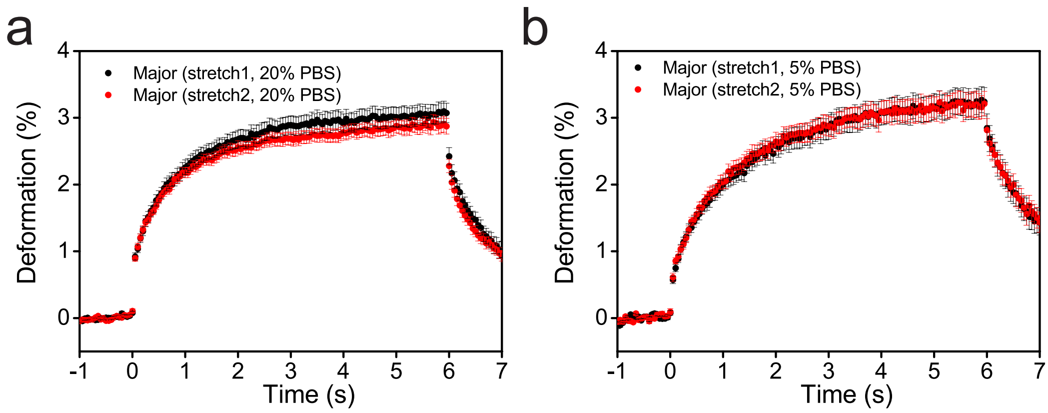

Fig. S6: Repeat heating experiments on HL60 nuclei in 780 nm OS. Major deformation profiles for HL60 nuclei in 20% PBS (**a**, n = 108) and 5% PBS (**b**, n = 108), during the first (black) and second stretch (red). Stretch periods are from $t = 0$ to 6 s. Both are prepared in deionized water, but heating is still minimal in the 780 nm OS (stretch power = 1.6 W, $\Delta T_{laser} \approx 3$°C). The deformation profiles overlap with each other indicating that the TIVT is highly reversible with no visible hysteresis. Error bars represent SE.

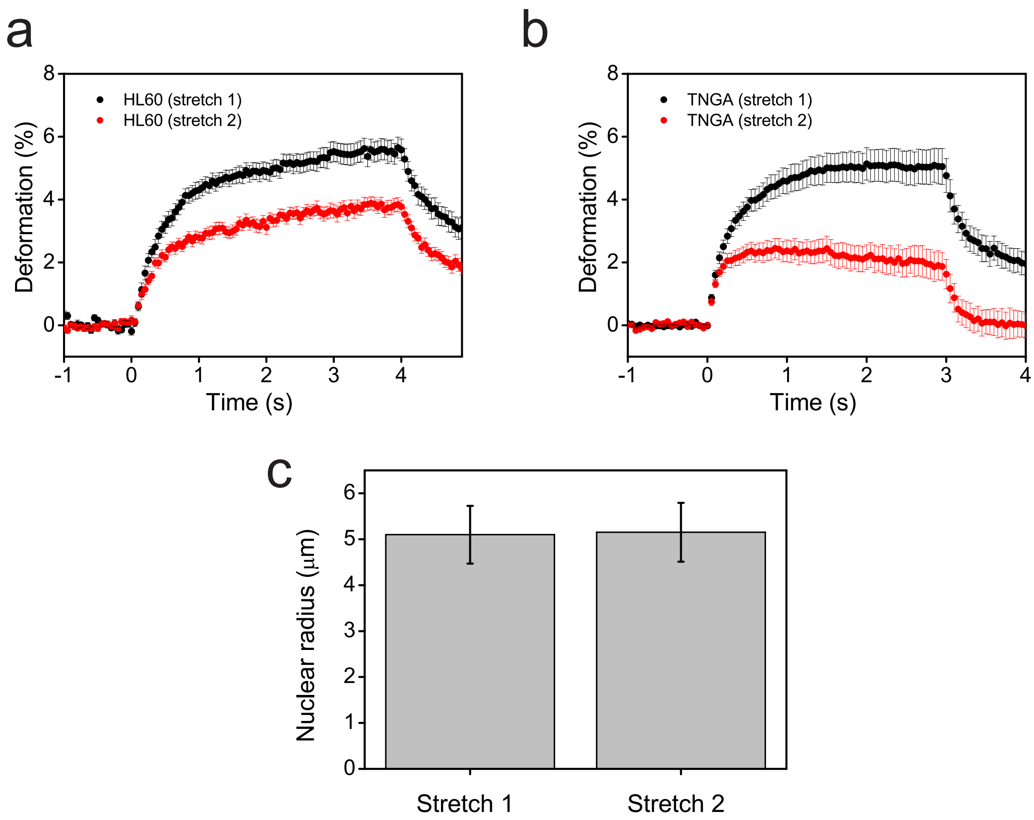

Fig. S7: Repeat heating experiments on isolated nuclei in 1064 nm OS. Deformation profiles along the major axis, for **a**. HL60 nuclei (n = 32, heating period t = 0 to 4 s), and **b**. TNGA nuclei (n = 18, heating period t = 0 to 3 s) during the first (black) and second stretch (red). Heating was more pronounced (stretch power = 1.6 W, $\Delta T_{laser} \approx 18°C$). **c**. Comparison of the initial nuclear size before the start of each stretch. The lack of a difference in the initial size suggests that the reduced amount of TIVT is not due to incomplete relaxation of nuclei and nuclear pre-strain before the next stretch. Error bars denote SE.

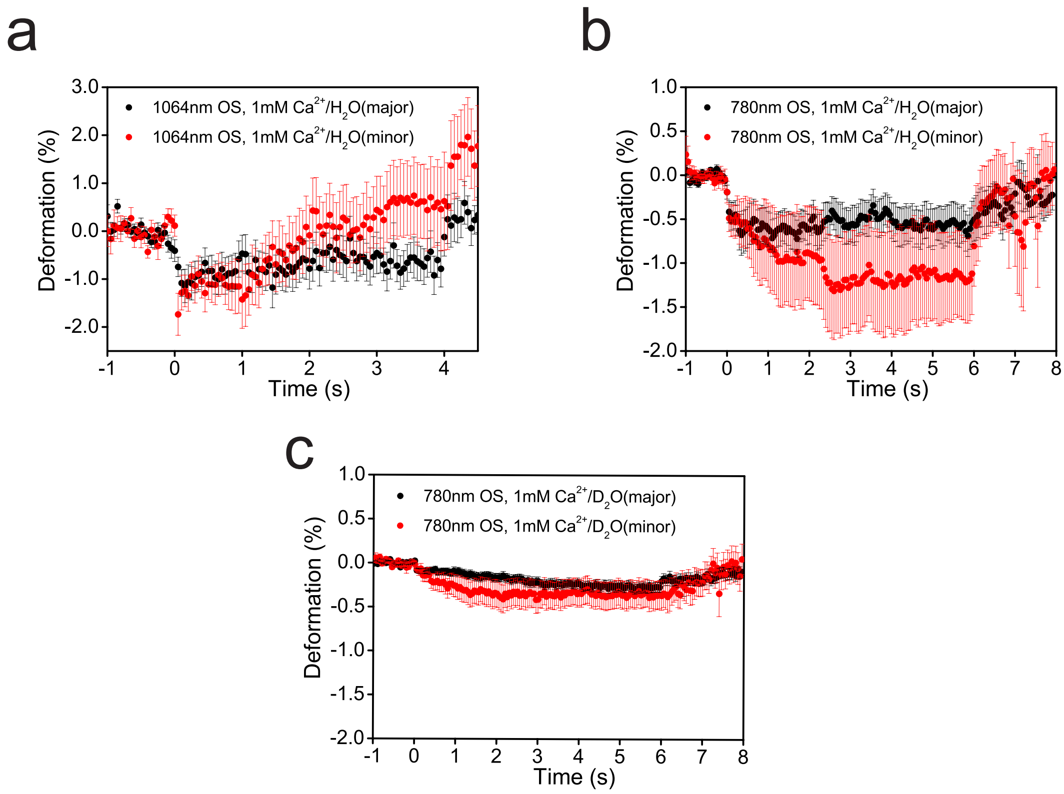

Fig. S8: Temperature induced nuclear contraction in multivalent salts correlates with the amount of transient heat. Deformation profiles for HL60 nuclei in **a.** 1 mM of $CaCl_2$ under optical stretching in 1064 nm OS (n = 17, $\Delta T_{laser} \approx 18°C$, stretch period t = 0 to 4 s), **b.** 1 mM of $CaCl_2$ (deionized water) in 780 nm OS (n = 17, $\Delta T_{laser} \approx 3°C$, stretch period t = 0 to 6 s), and **c.** 1 mM of $CaCl_2$ (heavy water) in 780 nm OS (n = 89, $\Delta T_{laser} \approx 1°C$, stretch period t = 0 to 6 s). Contraction along both axes is less pronounced with decreased laser-induced heating. Error bars denote SE.

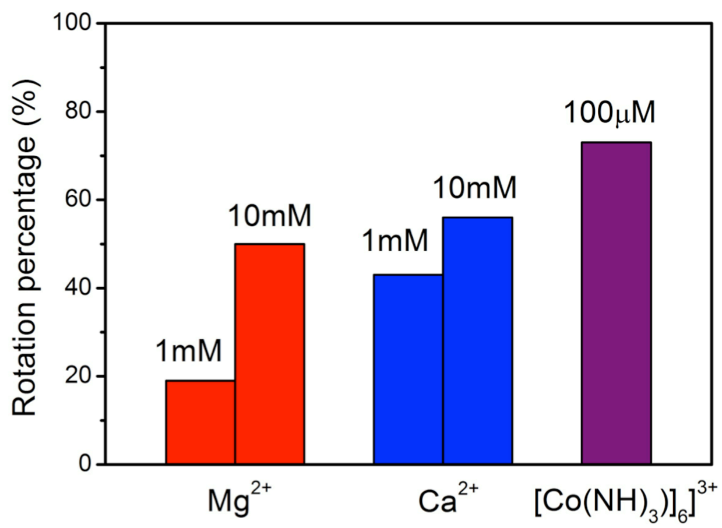

Fig. S9: Rotation statistics of nuclei under optical stretching in various multivalent salt concentrations. Higher concentrations of multivalent salts led to more nuclear rotations, with higher valency ions exerting a stronger effect. More than 30 nuclei are analyzed for each experimental condition.

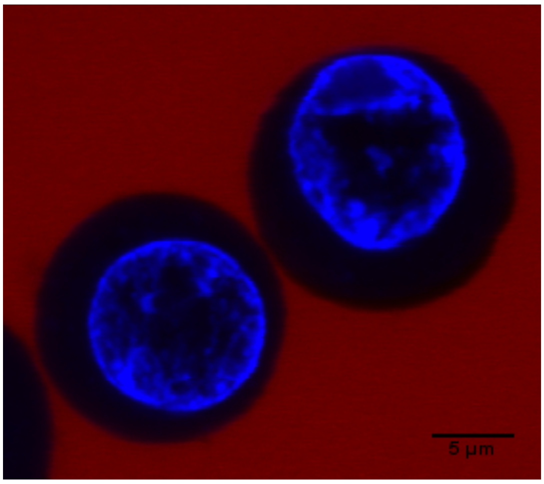

Fig. S10: Chromatin distribution in HL60 cells. Confocal composite image of HL60 cells stained for nucleus (Hoechst, blue) in PBS filled with rhodamine labeled 70 kDa (red) dextran. Pronounced compartmentalization of chromatin to the nuclear periphery was observed *in situ*, similar to those observed in isolated HL60 nuclei *in vitro*.

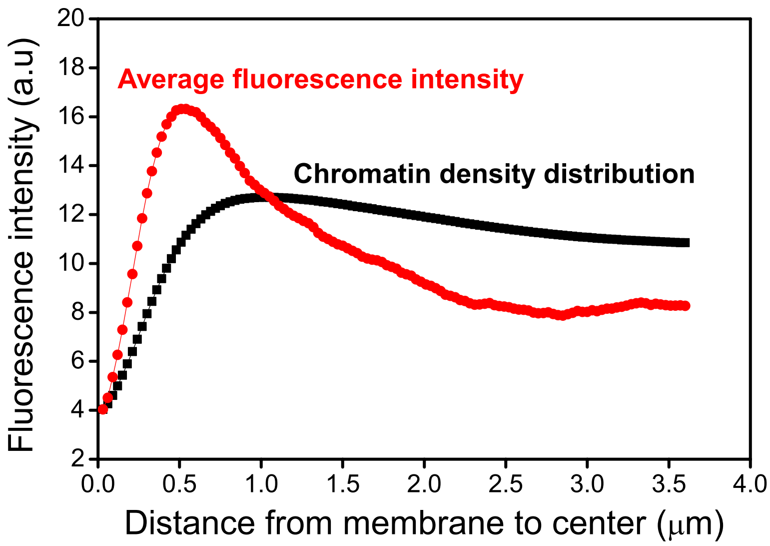

Fig. S11: Quantification of cortical chromatin distribution via fluorescence intensity profile analysis. The plots depict representative profiles (single nucleus) of the average fluorescence intensity and integrated intensity versus distance from the nuclear membrane to the center of the nucleus.

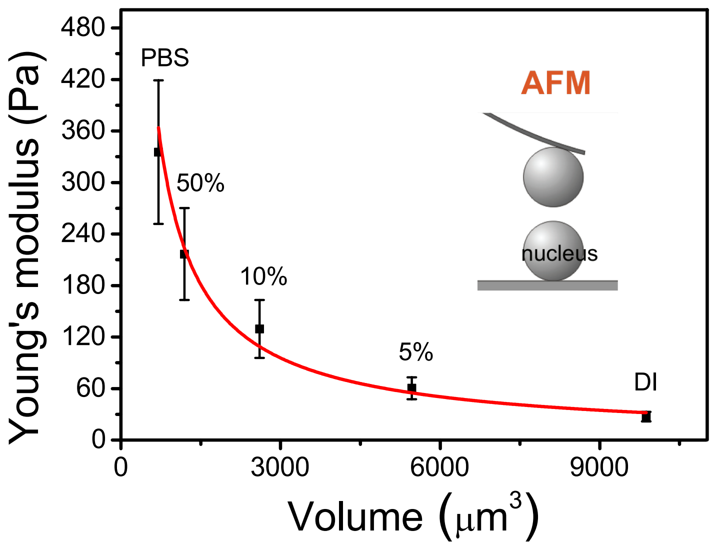

Fig. S12: AFM measurements of cortical chromatin stiffness for HL60 nuclei. Apparent stiffness of isolated HL60 nuclei swollen to various sizes, measured by AFM. Error bars denote SD. The measured values of the average Young's moduli are 335.4 ± 83.6 Pa, 216.7 ± 53.7 Pa, 129.4 ± 33.8 Pa, 60.3 ±12.7 Pa, and 27.4 ± 5.6 Pa for nuclei in PBS, 50% PBS, 10% PBS, 5% PBS and deionized water, respectively. The red curve denotes a fit based on the allometric model: $E = 1.7 \times 10^5 V^{-0.938}$ Pa. Adjusted goodness of fit $R^2 = 0.957$ indicates a good agreement with the measured data. More than 50 nuclei were analysed for each data point.

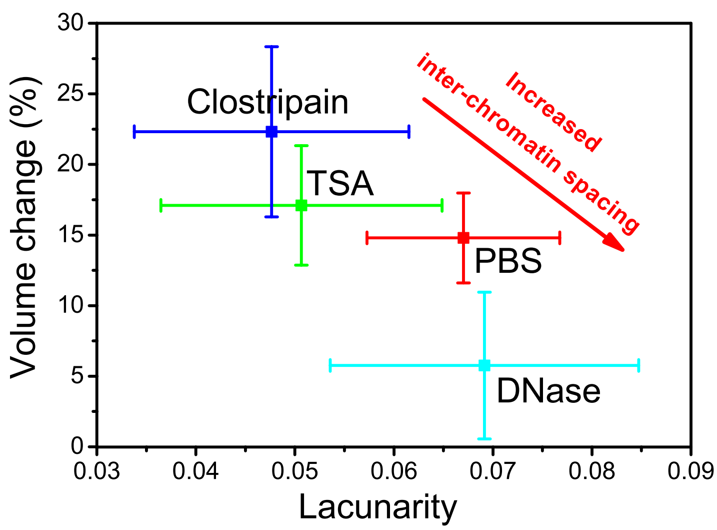

Fig. S13: Temperature-induced volume changes of nuclei versus lacunarity under pharmacological treatments. Lacunarity measures the texture and the distribution of voids in an image. Higher lacunarity indicates more voids or 'gappiness' in the image. The lacunarity of the nucleus significantly decreased under histone modifications (TSA, $n = 44$) and proteolysis (clostripain, $n = 27$), indicating that chromatin decondensation leads to a shrinkage of the pores and channels interdigitating the chromatin domains. Nuclei in PBS ($n = 21$) and DNase ($n = 17$), on the other hand, revealed higher lacunarity indicating uneven distribution of chromatin punctuated by dark, chromatin-free pores. Error bars denote SD.

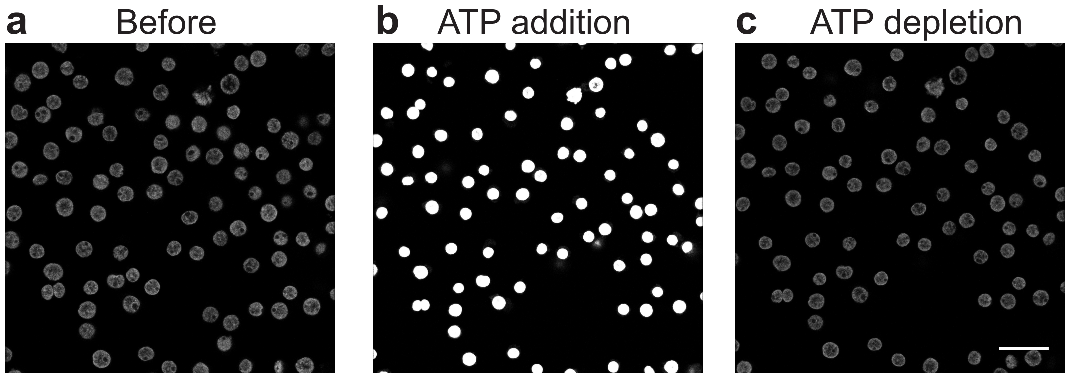

Fig. S14: Reversibility of chromatin condensation state induced by ATP. Confocal images of Hoechst stained HL60 nuclei in PBS buffer (**a**), followed by addition of ATP (**b**), which induces chromatin compaction and nuclear stiffening. Subsequent ATP depletion (**c**) further decondenses the chromatin, which correlates with nuclear softening against TIVT during optical stretching. Data was collected with identical microscope settings. Scale bar denotes 40 µm.

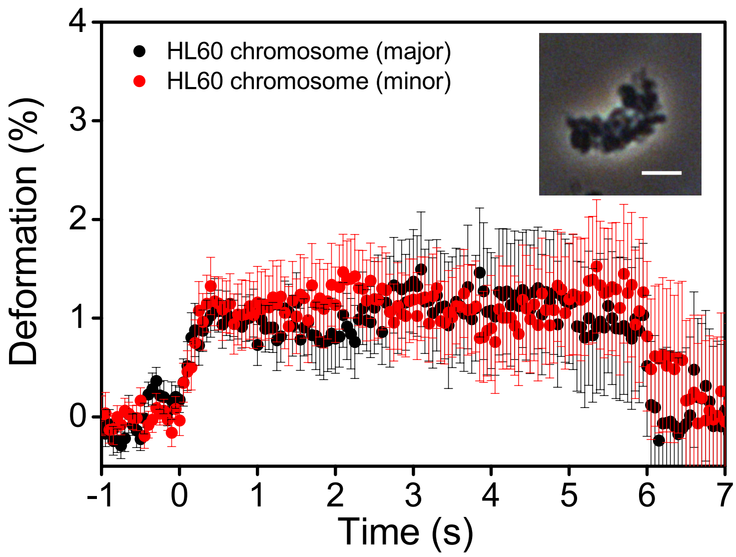

Fig. S15: HL60 mitotic chromosomes exhibit swelling under optical stretching in 1064 nm OS. Deformation curves for isolated HL60 chromosomes (n = 34), when stretched with 2.0 W ($\Delta T_{laser} \approx 23$°C) between t = 0 and 6 s. Inset depicts a phase contrast image of isolated chromosome. Error bars denote SE. Scale bar 5 µm.

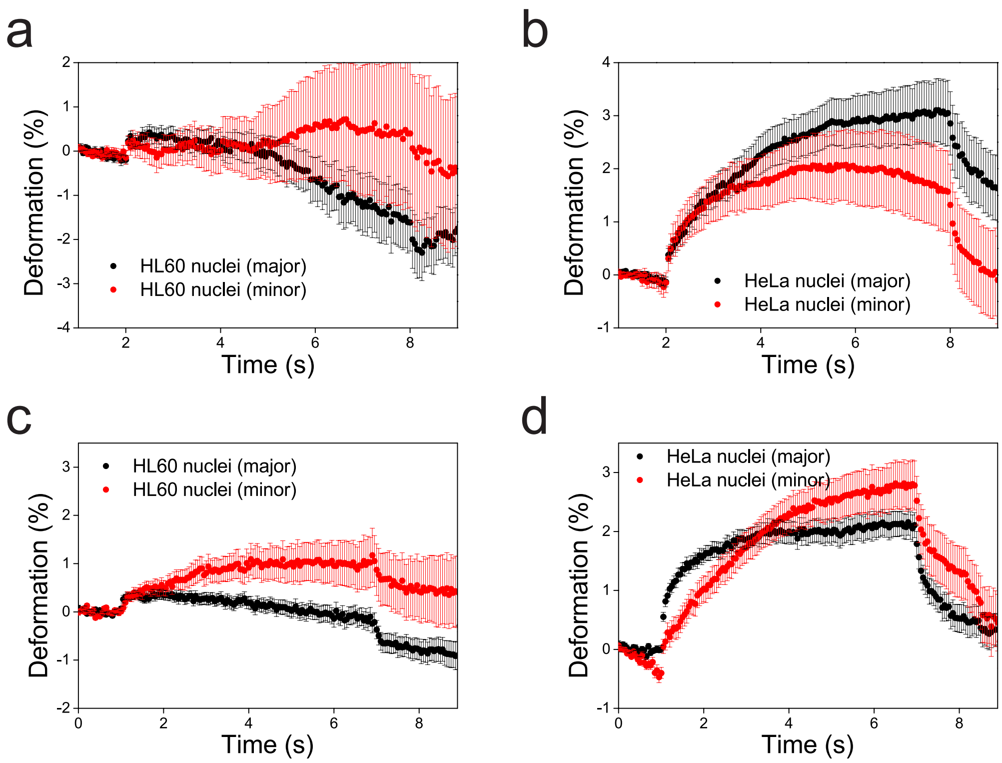

Fig. S16: Nuclear deformation *in situ* in OS. Nuclear deformation for a) HL60 (n = 31) and b) HeLa cells (n = 61), in an 1064 nm OS ($\Delta T_{laser} \approx 22°C$). Similar nuclear deformation profiles were observed for c) HL60 (n = 42) and d) HeLa nuclei (n = 51) *in situ* when stretched in an 780 nm OS in PBS prepared in D_2O ($\Delta T_{laser} \approx 1°C$).

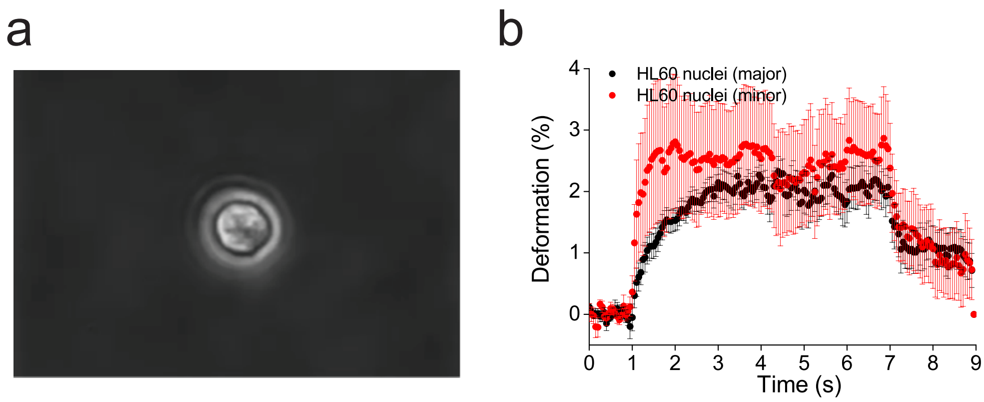

Fig. S17: a) Phase contrast image of isolated HL60 nuclei in 35 kDa PEG solution, under optical heating in 780nm OS. b) Average deformation profiles for a), when the nuclei (n = 11) are stretched with a total power of 1.6W and $\Delta T_{laser} \approx 3°C$. Stretch period is between t = 1 to 7 s. Error bars represent SE.

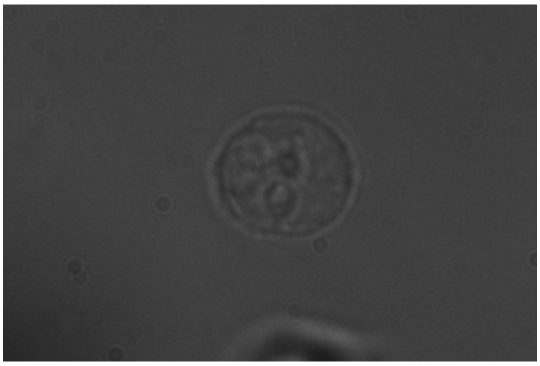

Movie. S1: Nuclear swelling in monovalent salts under optical stretching. Isolated HL60 nuclei swell in the presence of 100 mM of NaCl during TIVT. Laser power = 1.6 W, $\Delta T_{laser} \approx 18°C$. (WMV)

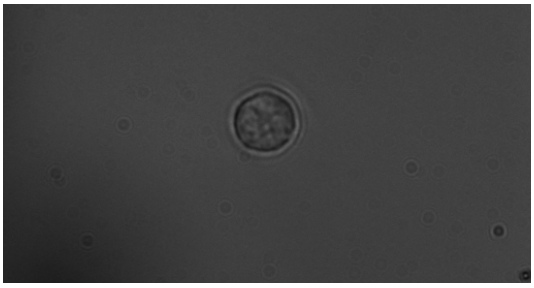

Movie. S2: Nuclear contraction in high concentrations of multivalent salts under optical stretching. Isolated HL60 nuclei contract in the presence of 10 mM of $MgCl_2$ during TIVT. Laser power = 1.6 W, $\Delta T_{laser} \approx 18°C$. (WMV)

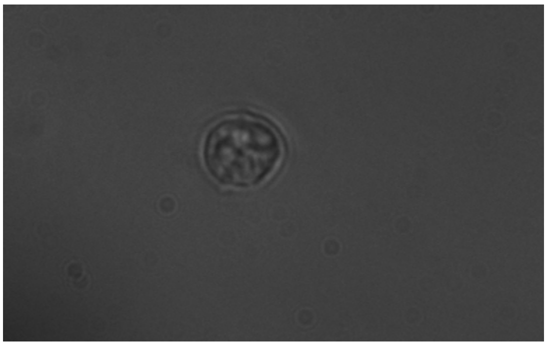

Movie. S3: Nuclear rotation in high concentrations of multivalent salts under optical stretching. Isolated HL60 nucleus can exhibit rotation along the major axis in 10 mM of $CaCl_2$ during TIVT. Laser power = 1.6 W, $\Delta T_{laser} \approx 18°C$. (WMV)